Table 2 Frequency comparison for the open isogrid paddle, Hz

Synthesis	Test	Mode shape
0.88	0.84	1st bending
3.95	3.94	1st torsion
4.21	4.16	2nd bending
11.11	11.83	2nd torsion
12.98	12.52	3rd bending
16.09	17.37	3rd torsion
19.00	20.55	4th bending

Table 3 Frequency comparison for the paddle of the ETS-V, Hz

	Test		
Synthesis	Free decay	Random	Mode shape
0.54	0.50	0.46	1st bending
2.03	1.22	1.20	1st torsion
1.95	2.15	2.20	1st in-plane
2.53	2.99	—	2nd bending
4.23	3.7	4.13	2nd torsion
6.08	—	—	3rd bending
8.38	—	—	2nd in-plane

the polynomials employed is

$$w = c_1 + c_2x + c_3y + c_4x^2 + c_5xy + c_6y^2 + c_7x^3 + c_8x^2y + c_9xy^2 + c_{10}y^3 + \cdots \quad (4)$$

The order of the polynomial depends on the number of mode measuring points, and it does not exceed the fourth order. The constants c_i are determined by the least-square approximation method. The rotational displacements $\partial w/\partial x$ and $\partial w/\partial y$ then can be derived directly by differentiating Eq. (4). The matrix $[\Phi]$ in Eq. (3) then can be enlarged by adding the terms $\partial w/\partial x$ and $\partial w/\partial y$ for each mode.

Application Examples

The synthesis method based on empirical data has been applied to two actual structures. One is an open isogrid structure shown in Fig. 1. The other is the paddle of the Japanese experimental testing satellite type V (ETS-V) shown in Fig. 2. These structures are divided into three parts and four joints (hinges). Each joint is modeled as a one-beam finite element whose stiffness parameters may be experimentally determined. Even if the whole structure is large, a vibration test of the two components combined with joints is possible in most cases. The synthesis procedure used is illustrated in Fig. 3. Note that damping terms are neglected. This is because, for the structures considered, the measured damping ratio is generally not accurate enough for damping synthesis. The component modes employed in the synthesis are summarized in Table 1. For components B and C, three rigid modes are included and theoretically obtained rigid modes are used. The synthesized results are compared with experimental results for the complete structure in Table 2 and Table 3. They are in good agreement except for the first torsional mode of the ETS-V. The cause of the disagreement is not in the synthesis algorithm itself, but in the poor test results of component A because it was difficult to secure a footing for excitation at a high ground in the test of component A of the ETS-V.

Conclusions

The component mode synthesis method based on measured modal data has been presented. The difficulty to provide the rotational displacements encountered in the synthesis is overcome by introducing polynomial approximation over the measured lateral displacement modes. The examples that have been presented demonstrate that the present method has potential as an alternative for modal tests of a complete structure.

References

[1]Craig, R. R., Jr., *Structural Dynamics—An Introduction to Computer Methods,* Wiley, New York, 1981, pp. 467–495.

[2]Charron, F., Sorocky, S. J., Jha, V. K., Vigneron, F. R., and Lapierre, H., "Substructure Coupling of Analytical and Test Models for an Experimental Structure," *Proceedings of the 4th International Modal Analysis Conference,* Vol. 2, Union College, Schenectady, NY, 1986, pp. 1463–1470.

[3]Sachs, W., "Identification of a Complex Satellite Model by Means of Modal Synthesis," *Proceedings of the Fifth International Modal Analysis Conference,* Vol. 1, Union College, Schenectady, NY, 1987, pp. 468–477.

Dynamic Evaluation of the NASA-ORNL Traction-Drive Joint

Clarence W. de Silva*
University of British Columbia, Vancouver, British Columbia, V6T 1W5 Canada
and
Walter W. Hankins III†
NASA Langley Research Center, Hampton, Virginia 23665

Introduction

SINCE conventional motors provide speeds that are too high for most robotic tasks and since high driving torques are desirable, speed reducers such as gear transmissions, timing belts, and sprocket and chain devices are usually incorporated at the manipulator joints. Gear transmissions can introduce backlash, which can result in low stiffness, degraded accuracy and repeatability, accelerated wear, noise and vibration, and dynamic and control problems, including limit cycle response. Backlash can be reduced using special gear designs. Harmonic drives, for example,[1] incorporate preloading at the tooth mesh region, but this can increase friction and local stresses. Direct-drive manipulators use high-torque, low-speed dc motors without gear reducers.[2,3] They are known to have low levels of joint friction and practically no backlash. Unfortunately, however, a direct-drive joint tends to be considerably heavier than a conventional joint having comparable capabilities. This would demand stronger and heavier links with associated reductions in bandwidth and increased flexibility problems.

Recently, the use of traction (friction) drive has been proposed as an alternative to gear transmission, and a manipulator using traction drives for the joints is being developed.[4] This drive promises improvements in the manipulator performance in terms of accuracy and efficiency. In particular, backlash problems would be virtually nonexistent and the frictional dissipation would be small. Furthermore, it has the potential for high stiffness and smooth operation, with overload protection naturally built into the joint through the friction-drive mechanism. However, traction drives are known to have two disadvantages. They are bigger and heavier than gear transmissions and practical experience with them is limited. This paper

Received May 10, 1989; revision received Aug. 24, 1989.

*NSERC Professor of Industrial Automation, Department of Mechanical Engineering.
†Engineer.

presents a dynamic analysis and evaluation of a traction-drive joint. A dynamic model is developed for the joint. Its behavior is evaluated using controllability, observability, stability, and response analyses. Next, the servo control problem of a single joint is studied in terms of the required outputs for the feedback servo and with regard to the optimal performance.

Laboratory Telerobotic Manipulator Model

NASA Langley Research Center is currently sponsoring construction of a laboratory telerobotic manipulator (LTM) by the Department of Energy's Oak Ridge National Laboratory (ORNL).[4] The LTM will be able to be operated as a dual arm force-reflecting master/slave teleoperator or as a robot, using distributed high-speed microprocessors. The LTM has redundant kinematics, supplied by differential traction drives

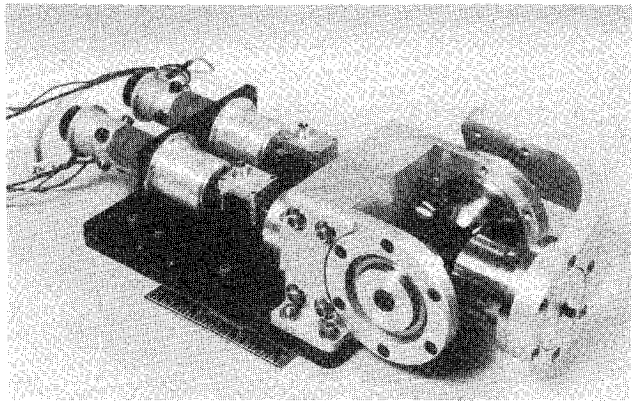

Fig. 1 Prototype traction-drive mechanism (NASA-ORNL).

at the shoulder, elbow, and wrist joints, plus a seventh (roll) degree of freedom at the wrist. Figure 1 shows a traction-drive differential test fixture. The two input rollers are frictionally engaged with two intermediate wheels of much larger diameter, which form a differential mechanism. These two differential wheels are, in turn, frictionally engaged with a single output roller. When the two differential wheels rotate in opposite directions at the same speed, the output roller will undergo a roll motion about its axis. When the two differential wheels rotate in the same direction at equal speeds, the output roller will pitch without any rolling motion. In this manner, two degrees of freedom are provided by a single joint. Note that the roll motion of the output roller can be interpreted as a yaw motion if the output shaft is bent through 90 deg. Also, any combination of yaw and pitch motions can be produced at the output of the joint simply by adjusting the motions of the two input rollers that are driven using dc servo motors. Digital shaft encoders for position (and speed) sensing, tachometers for analog speed sensing, and torque sensors[1] are incorporated in each axis. These sensors will provide the feedback signals for the operation of the joint servo.

The traction-drive joint described in the previous section[1] may be modeled as in Fig. 2. Motor torques, not drive voltages, are used as the inputs to the joint. The rationale here is that the coupling of the motor back emf can be compensated by using a local current feedback loop in the drive amplifier. The Lagrange energy method is used to establish the dynamic equations for the joint. Joint backlash is neglected, and energy dissipation is modeled as viscous damping. Flexibility of the input drive roller is represented by a torsional stiffness K. Other moving components are individually assumed to be rigid. The moment of inertia of each such component is denoted by J, with a suitable subscript. Each inertia component

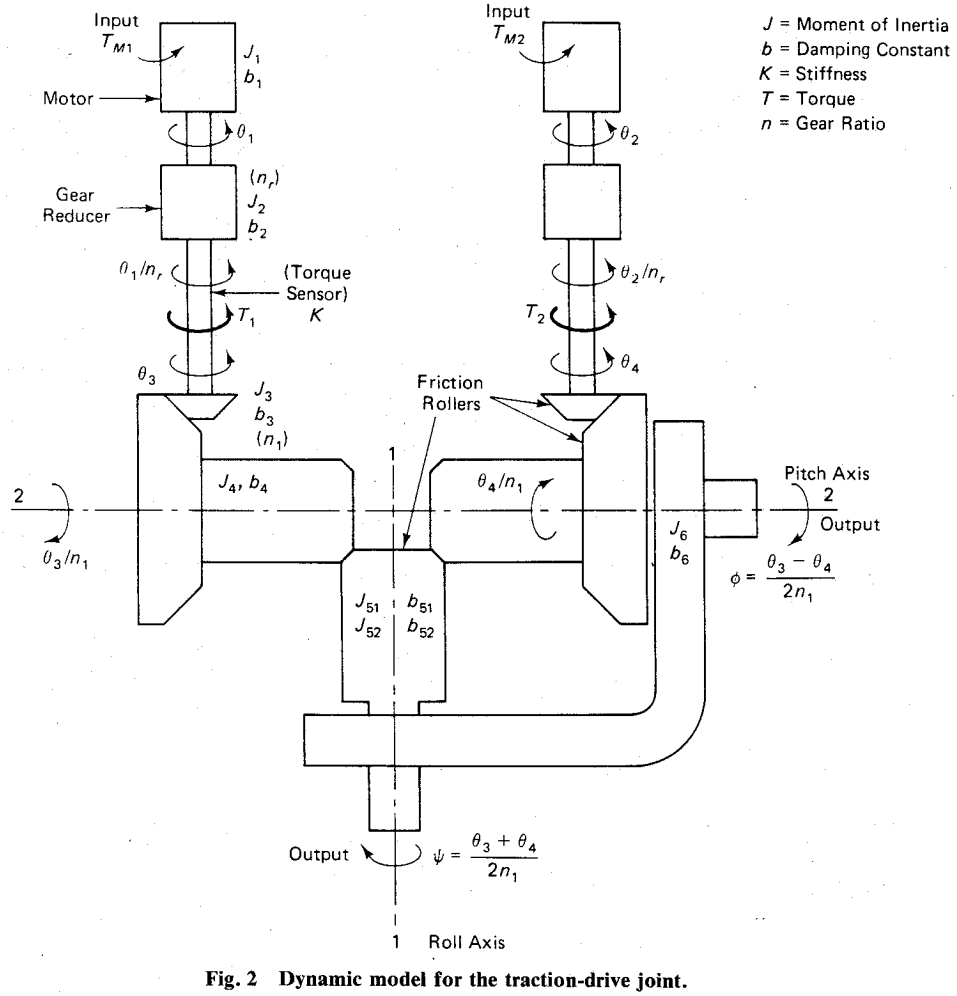

Fig. 2 Dynamic model for the traction-drive joint.

will also have an associated damping constant that is denoted by b with the same subscript. Suppose that J_1 = combined inertia of motor rotor and drive side of the speed reducer, J_2 = combined inertia of the driven side of the speed reducer and input side of the drive roller, J_3 = inertia of the output side of the drive roller, and J_4 = inertia of one differential wheel.

The output member has two axes of rotation, denoted as roll axis and pitch axis in Fig. 2. This member actually consists of two rigid components. The output shaft that is directly engaged with the differential wheels has an inertia J_{51} about the roll (yaw) axis and an inertia J_{52} about the pitch axis. The cross member transmits the pitch motion of the output shaft and it has a pitch inertia of J_6. This member does not undergo a roll (yaw) motion. It follows that by considering the two orthogonal axes of motion (roll and pitch), the inertia matrix of the combined output member may be expressed in which J_c is the cross inertia that represents the inertial coupling between the two axes, resulting from the fact that the roll axis and the pitch axis are not the principal axes of inertia of the output member, in general.

Suppose that θ_1 and θ_2 denote the angles of rotation of the two motors, and θ_3 and θ_4 are the angles of rotation at the output ends of the drive rollers, as indicated in Fig. 2. If n_R is the gear ratio of the speed reducer, the rotations at the input ends of the drive rollers will be θ_1/n_R and θ_2/n_R as shown. Also, θ_3/n_1 and θ_4/n_1 will be the rotations of the differential wheels, n_1 being the transmission ratio from the drive roller to the differential wheel. Assuming the transmission ratio from the differential wheels to the output member to be unity along both roll and pitch axes, we observe that the roll (yaw) angle is

$$\psi = (\theta_3 + \theta_4)/2n_1 \tag{1}$$

and the pitch angle is

$$\phi = (\theta_3 - \theta_4)/2n_1 \tag{2}$$

First, for brevity, define the following parameters:

$$J_{1eq} = J_1 + (J_2/n_R^2) \tag{3}$$

$$J_{2eq} = J_3 + (J_4/n_1^2) + (J_{51} + J_{52} + J_6)/4n_1^2 \tag{4}$$

$$J_{3eq} = (J_{52} + J_6 - J_{51})/4n_1^2 \tag{5}$$

$$J_{ceq} = J_c/2n_1^2 \tag{6}$$

Also, b_{1eq}, b_{2eq}, and b_{3eq} are defined in an analogous manner. Then, using the standard Lagrange formulation, the dynamic equations for the joint can be written as

$$J_{1eq}\ddot{\theta}_1 + b_{1eq}\dot{\theta}_1 + (K/n_R^2)\theta_1 - (Kn_1/n_R)(\psi + \phi) = T_{m1} \tag{7}$$

$$J_{1eq}\ddot{\theta}_2 + b_{1eq}\dot{\theta}_2 + (K/n_R^2)\theta_2 - (Kn_1/n_R)(\psi - \phi) = T_{m2} \tag{8}$$

$$(J_{2eq} - J_{3eq})\ddot{\psi} + J\ddot{\phi} + (b_{2eq} - b_{3eq})\dot{\psi} + K\psi - (K/2n_1n_R)(\theta_1 + \theta_2) = 0 \tag{9}$$

$$(J_{2eq} + J_{3eq})\ddot{\phi} + J\ddot{\psi} + (b_{2eq} + b_{3eq})\dot{\phi} + K\phi - (K/2n_1n_R)(\theta_1 - \theta_2) = 0 \tag{10}$$

These equations represent a coupled, four-degree-of-freedom, eighth-order model with two inputs T_{m1} and T_{m2}. An assumption that would considerably simplify a state-space formulation is that J_{ceq} is negligible in comparison to the remaining inertia parameters. This assumption is justified here because the cross inertia term J_c is usually small compared to the direct inertia terms and because the transmission ratio n_1 is larger than unity.

The state vector x is defined as $x = [\theta_1, \dot{\theta}, \theta_2, \dot{\theta}_2, \psi, \dot{\psi}, \phi, \dot{\phi}]^T$ and the input vector u is given by $u = [T_{m1}, T_{m2}]^T$. Torques transmitted through the two drive rollers, as measured by the torque sensors, and the roll (yaw) angle and the pitch angle, as measured by the roll and pitch encoders, are taken as the system outputs:

$$y_1 = T_1 = K(\theta_1/n_R - \theta_3) = K(x_1/n_R - n_1x_5 - n_1x_7) \tag{11}$$

$$y_2 = T_2 = K(\theta_2/n_R - \theta_4) = K(x_3/n_R - n_1x_5 + n_1x_7) \tag{12}$$

$$y_3 = \psi = x_5 \tag{13}$$

$$y_4 = \phi = x_7 \tag{14}$$

Performance Evaluation

Parameter values were chosen in consultation with ORNL and product data sheets to represent the true inertia, stiffness, and damping properties of the joint. The following values are used: $J_1 = 0.28$, $J_2 = 0.49$, $J_3 = 0.21$, $J_4 = 0.70$, $J_{51} = 5.6$, $J_{52} = 2.8$, and $J_6 = 3.5$ all in units of 1×10^{-3} kg·m^2; $b_1 = b_3 = b_4 = b_{51} = b_6 = 21.0$, $b_2 = 28.0$ all in units of 1×10^{-6} N·m/rad/s; $n_R = 30$; $n_1 = 3.75$, and $K = 210.0$ N·m/rad. A commercially available software package for analysis and design of control systems was used in the studies to be described. First the joint model was programmed into the system using the DIARY capability of the software package. Next controllability, observability, stability, and response studies were conducted. Finally control studies were performed.

For the joint model developed here, it was verified that the controllability condition is satisfied. This means that we should be able to realize any joint response that we desire or be able to control the joint in any manner by using appropriate inputs. If all eight states of the model can be measured and used in controlling the joint, it is known that the joint can be controlled in an optimal manner, and that stability of the system can be improved in an arbitrary manner. But it is not always possible or convenient to measure all state variables in a system. Then the question arises whether it is possible to determine the value of the state vector at any arbitrary instant by measuring the output vector from that instant for a finite period of time. The system is said to be observable if and only if this is possible. It was verified that the traction-drive joint, as defined previously, is observable. It follows that output feedback can be structured for complete-state feedback without compromising the joint performance. It can be concluded that the four outputs defined in the state model are quite adequate for "servoing" the joint.

Further study revealed that the system is observable with the two motion variables (roll and pitch angles) alone. This indicates that the torque sensing is not needed, in theory, to completely control the joint. In practice, however, torque sensing might be quite useful. For example, a hybrid control scheme consisting of both motion feedback and torque feedback could considerably improve the performance of the joint under load disturbances, unknown parameters, and when the fine manipulation under very tight motion tolerances is needed, as in the case of parts assembly or in manipulations under motion constraints where damaging forces could arise even with small motion errors. It was found that the system is not completely observable when only one of the two motion variables is measured. In this case, only four of the eight state variables can be estimated. It follows that roll angle and pitch angle both are needed for servoing the joint.

Stability is determined by the eigenvalues of the system matrix. Without any feedback control, the eigenvalues are found to be $-0.03 \pm j677.10$, $-0.02 \pm j659.48$, -0.07, -0.07, 0.0, 0.0. It is noted that the open-loop system is marginally stable, as indicated by the zero eigenvalues. This is to be expected in view of the fact that the joint is driven by two

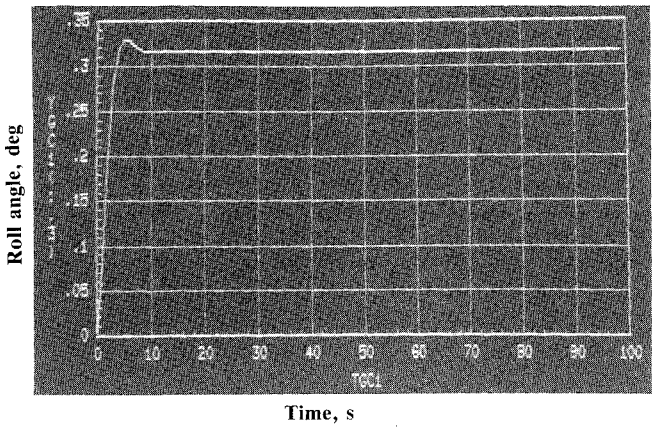

Fig. 3a Step response of the roll angle under feedback control.

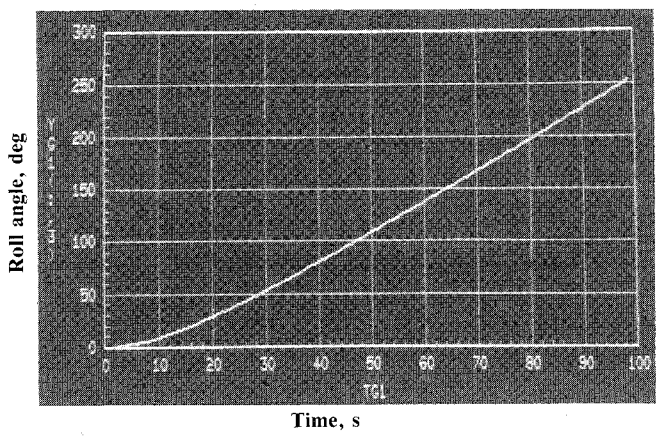

Fig. 3b Step response of the roll angle of the output member.

actuators, each of which have a characteristic equation of the form $s(s + 1)$. Feedback control is needed to stabilize the joint. This is provided by measuring the outputs and feeding them through constant gain amplifiers—the typical servo configuration.

Several simulation runs were carried out in order to study the open-loop response of the joint. Unit step inputs of motor torques were used throughout. As expected, when the motor torques were equal in magnitude and direction, the response was found to be a pure roll motion at the output member without any pitch motion. Similarly, when the motor torques were equal in magnitude but opposite in direction, the output member underwent a pure pitch motion without any roll motion. For other combinations of torque inputs, both roll and pitch motions were simultaneously present. These observations confirm the behavior that is expected from the actual joint.

The slope of the angular response curve becomes constant eventually. This is the steady-state condition of constant speed. Under this condition, the torques at various locations of the joint are utilized exclusively to overcome damping. Damping torques are distributed in such a manner that large torques appear at high-speed components of the traction drive and small torques at low-speed components. Accordingly, with the speed ratios used in the present simulation, most of the damping torque will be concentrated near the two motors. Initially a large torque is needed to accelerate the low-speed components such as the output side of the drive rollers, but eventually these torques will settle down to small values. If the speed reductions are eliminated, the torque distribution will become more uniform. For example, results obtained using $n_R = 1$ and $n_1 = 1$, and for a motor torque of 7×10^{-3} N · m indicated that, in this case, the torque at the drive roller output reaches a peak of about 8.4×10^{-3} N · m and eventually settles down to a value of about 3.5×10^{-3} N · m. Naturally, the speed distribution will also depend on the values of n_R and n_1.

Several more simulations were carried out to study the effects of other types of parameters on the joint response. Notably, when damping is increased, the steady-state roll and pitch speeds reduce in proportion. In particular, if all damping constants are increased by a factor of 10 while keeping the other parameters the same, the eigenvalues of the open-loop system become $-0.25 \pm j677.10$, $-0.25 \pm j659.48$, -0.75, -0.75, 0.0, 0.0. Note that the stable eigenvalues have become more stable, whereas the zero eigenvalues are not affected. In particular, the real parts of the eigenvalues have increased by approximately a factor of 10, whereas the natural frequencies are virtually unchanged. The torque distribution will also be affected by this, large increases being noted at high-speed components.

When the stiffness of the drive rollers is decreased, the primary frequency of the torque response decreases, whereas the roll- and pitch-motion responses remain almost unaffected. For example, if the stiffness is decreased by a factor of 10 (i.e., $K = 21.0$ N · m/rad) keeping the other parameter values unchanged, the open-loop eigenvalues of the joint become: $-0.03 \pm j214.12$, $-0.02 \pm j208.55$, -0.07, -0.07, 0.0, 0.0. Here the natural frequencies of the complex eigenvalues have been reduced by a factor of approximately $\sqrt{10}$, whereas the real eigenvalues are not influenced. It follows that the natural frequencies of the joint are directly affected by the stiffness of the drive rollers.

To illustrate the level of improvement that is realizable under servo control, a linear quadratic regulator (LQR) is designed for the joint using complete state feedback. A similar performance level is possible with feedback of the roll and pitch angles alone because the states are completely observable even with these two outputs.

The weighting matrices used in the performance index are

$$\boldsymbol{R}_x = \text{diag}(0.0,\ 0.0,\ 0.0,\ 0.0,\ 1.0,\ 0.0,\ 1.0,\ 0.0)$$

$$\boldsymbol{R}_u = \text{diag}(0.05,\ 0.05)$$

When this controller is included in the joint, the step response of the roll angle becomes as shown in Fig. 3a. This should be compared with the open-loop step response shown in Fig. 3b, which was obtained under the same (step) torque input. In particular, good rise time has been achieved without introducing a large overshoot. Also, fast settling to the steady-state angle is seen. The eigenvalues of the closed-loop joint are computed to be $-0.03 \pm j677.10$, $-0.02 \pm j659.48$, $-0.59 \pm j0.59$, $-0.59 \pm j0.59$. Note that the free integrators in the open-loop joint have been modified to a stable pair of complex eigenvalues. The stable pair of real eigenvalues in the open-loop joint has also been transformed into a stable complex pair. It can be concluded that satisfactory performance of the traction-drive joint would be possible with a suitable joint servo using at least roll- and pitch-angle feedback.

The foregoing study reveals that a traction-drive unit can provide a reasonably well-behaved manipulator joint. Independently operating, each joint will behave in a desired manner under servo control. When several such joints are used in a single robot, there will be unavoidable dynamic coupling among joints. Due to these interactions, accurate performance of the manipulator will not be possible, in general, if the joints are controlled independently. Dynamic performance of the manipulator can be improved by employing a control scheme that takes into account dynamic interactions among joints. Another factor that would need attention is the nonlinear nature of the manipulator.

Acknowledgments

The work reported in this paper was carried out at NASA Langley Research Center under a NASA-American Society for Engineering Education Fellowship awarded to C. W. de Silva.

References

[1]De Silva, C. W., *Control Sensors and Actuators*, Prentice-Hall, Englewood Cliffs, New Jersey, 1989.

[2]Asada, H., and Youcef-Toumi, K., "Analysis and Design of a Direct-Drive Arm with a Five-Bar-Link Parallel Drive Mechanism," *Proceedings of the 1984 American Control Conference*, Inst. of Electrical and Electronics Engineers, Piscataway, NJ, June 1984, pp. 1224–1230.

[3]Kanade, T., and Schmitz, D., "Development of CMU Direct-Drive Arm III," Robotics Institute of Carnegie Mellon University, Pittsburgh, PA, Rept. CMU-RT-TR-85-5, March 1985.

[4]Martin, H. L., Kuban, D. P., Herndon, J. N., Williams, D. M., and Hamel, W. R., "Recommendations for the Next-Generation Space Telerobot System," Oak Ridge National Laboratory, Oak Ridge, TN, Rept. ORNL/TM-9951, March 1986.

Model Reduction for Flexible Structures: Test Data Approach

Wodek Gawronski*
Jet Propulsion Laboratory,
California Institute of Technology,
Pasadena, California 91109

Introduction

OBTAINING a reasonable reduced model for a flexible structure (a system with separated complex poles and small damping) is an important task for an analyst as well as a test engineer. This task has been satisfactorily solved for analytical models of a flexible structure; however, the reduction of a model of a flexible structure obtained from test data has not yet been considered. In this Note, two important questions are solved that can help one to use resonance test data in model reduction.

A reduced model is obtained by truncating part of the state variables. The reduction indices determine which component is deleted or retained in the reduced model. The indices are obtained from the transfer function (in the form of resonance test data), rather than from the system matrices.

Test data, besides system dynamics, also include actuator and sensor dynamics. The reduced model obtained from these data can be far from the optimal because it includes unwanted actuator-sensor dynamics. In this Note, the reconstruction of the flexible structure indices from the joint actuator-sensor-flexible structure indices is discussed and illustrated.

Reduction Indices from Test Data

There are two indices used in model reduction: Hankel singular values of Moore[1-4] and component costs of Skelton.[3-6] The Hankel singular value γ_i, a simultaneous measure of controllability and observability of the ith state coordinate, is determined in the balanced coordinates. In this case the reduced system is obtained by deleting the least controllable and observable states.

Component cost σ_i is a norm of the ith component. For uncoupled coordinates, the norm of the output is a sum of norms of each component. This approach has proved to be quite successful when modal coordinates, which are almost always uncoupled, are used.

Received April 12, 1989; revision received Oct. 25, 1989.

*Member, Technical Staff, Ground Antennas and Facilities Section. Member AIAA.

It is well known that flexible structures with small damping and separated poles have controllability and observability grammians that are diagonally dominant[1] [$W_c \approx \text{diag}(W_{ci})$, $W_0 \approx \text{diag}(W_{0i})$], where, from Ref. 3,

$$W_{ci} = I_2(||b_i||^2/4\zeta_i\omega_i), \qquad W_{0i} = I_2(Y_i^2\zeta_i\omega_i/||b_i||^2) \tag{1}$$

and Y_i is the norm of the output at ith natural frequency (see the Appendix). For these structures, the balanced grammians are obtained simply as $W_{cb} = W_{0b} = (W_cW_0)^{1/2} = \text{diag}(W_{bi})$, and from Eq. (1) one obtains $W_{bi} = I_2Y_i/2 = I_2Y^2$. This shows that for flexible structures the square of the ith Hankel singular value is equal to one-half of the norm of the output at the ith resonance:

$$\gamma_i = 0.5Y_i \tag{2}$$

Figure 1 shows the determination of γ_2 from the resonance test data for a single-input/single-output system:

$$\gamma_2 = 0.5Y_2 = 0.5||H(\omega_2)||$$

The cost of the ith modal coordinate is determined from Ref. 4:

$$\sigma_i^2 = \text{tr}(A_i\gamma_i^2) = 0.5\zeta_i\omega_iY_i^2 \tag{3}$$

where A_i is given in the Appendix. Denoting the half power frequency[7] $\Delta_i = 2\zeta_i\omega_i$ (see Fig. 1), one can rewrite Eq. (3) as

$$\sigma_i = 0.5Y_i\sqrt{\Delta_i} = \gamma_i\sqrt{\Delta_i} \tag{4}$$

Unlike Hankel singular values, the cost consists of a product of the resonance amplitude and the resonance width.

As an example, the flexible structure in Fig. 2 with 42 state variables, single input and single output, is considered. Sensors and actuators are placed so that all Hankel singular values are equal ($\gamma_i = 1$, $i = 1,\ldots, 42$); i.e., all states are equally controlled and observed. The plots of Hankel singular values are given in Fig. 3. The analytical Hankel singular values (solid line) and those obtained from the transfer function (dotted line) are nearly the same, especially for $nr < 16$.

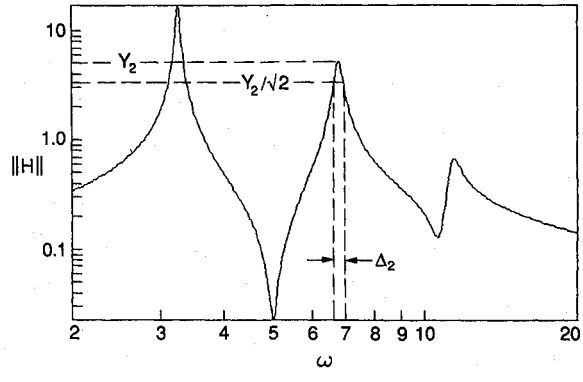

Fig. 1 Hankel singular value and component cost from resonance test.

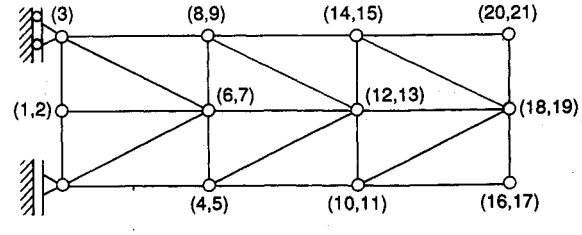

Fig. 2 Flexible structure.